

# Fourier imaging of uncladded fibres using a liquid wedge interferometer

A. M. HAMED

Physics Department, Faculty of Science, Ain Shams University, Cairo, Egypt.

The intensity distribution of a Gaussian laser beam passing through uncladded fibre, immersed in a liquid wedge, is obtained. The Airy distribution modulated by the Gaussian beam and the fibre function is deduced from the intensity distribution of the liquid wedge. Analytical formulae of sharpness and image contrast are obtained in the case of Gaussian distribution. Three curves of sharpness are plotted for different mirror reflectivities. The optical path difference, in the case of a liquid wedge provided with the uncladded fibre, is calculated.

## 1. Introduction

TOLANSKY [1] has carried out for the first time the analysis for the necessary conditions to produce multiple beam localized fringes using a liquid wedge interferometer. He has pointed out that the Airy's summation holds only for a parallel plate, but if certain conditions are fulfilled for a silvered air wedge, then a close approximation to the Airy summation can be achieved. In the case of a wedge, the successive multiple reflected rays are not behind each other in phase in exact arithmetic series, while in the case of plane parallel plates the path difference between any two successive rays is  $\lambda/2$ . The optimum condition for producing multiple beam localized fringes reached by Tolansky necessitates using a small wedge angle  $\alpha$  and a small interferometric gap to secure the Airy's sum conditions [2]. He considered the allowed limit for the retardation to be equal to  $\lambda/2$ , while BARAKAT *et al.* [3], [4] found that the permitted limit is  $3\lambda/8$ .

Many authors [5]–[14] have obtained interference fringes using synthetic optical fibres. They considered the problem from the geometrical point of view only, taking into account ray optics approximation. BARAKAT [5] obtained a right formula of multiple beam Fizeau fringes crossing a fibre of circular transverse section immersed in a silvered liquid wedge, considering ray optics. He determined the fringe shift of the fibre with respect to the trigonometric fringes ( $\delta z/\Delta z$ ), followed by others [6], [7] who extended the analysis to multilayer fibres. HAMZA *et al.* [8] determined the refractive indices and birefringence of fibres having irregular transverse sections of homogeneous fibres. BOGGET *et al.* [15], PRESBY *et al.* [16] described automated transverse interferometric method and deduced the index profile of graded index fibre.

In this study, we take into consideration the effect of the wedge angle  $\alpha$  upon the arithmetic series and use a Gaussian laser beam for the illumination of the inter-

ferometer. A theoretical analysis is presented based on Fourier techniques followed by theoretical results and, finally, a conclusion is given.

### 2. Theoretical analysis

The output of a He-Ne laser operating in the fundamental mode is considered as a Gaussian beam. Such a beam is incident upon a liquid wedge interferometer. We describe this beam in the plane  $z = z_1$  by an amplitude distribution of the form [17]

$$U_1(r) = A_1 \text{Gauss}(r/b_1) = A_1 \exp[-\pi(r/b_1)^2] \tag{1}$$

where  $b_1$  denotes the effective width of the beam and  $A_1$  describes the magnitude of the incident wave field,  $r$  – radial coordinate in the object plane  $(x, y)$ . The incident beam exhibits a displacement resulting from the multiple reflections occurring between the two plates of the wedge interferometer.

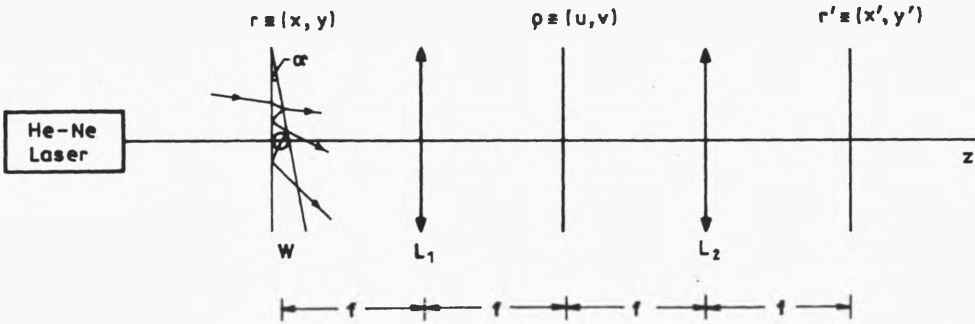


Fig. 1. Imaging system of multiple beam interference fringes obtained using a liquid wedge provided with uncladded fibre.  $W$  – liquid wedge interferometer,  $L_1$  – Fourier transform lens,  $L_2$  – imaging lens,  $F$  – uncladded fibre of circular cross-section

The resultant complex amplitude is obtained by taking the sum over all the transmitted rays after making the multiple reflections, as shown in Fig. 1; hence we can write

$$U'_1(r) = U_1(r)g(r)\{1 + r_1^2 \exp(jk\Delta) + r_1^4 \exp[jk(2\Delta + \epsilon_1)] + r_1^6 \exp[jk(3\Delta + \epsilon_2)] + \dots\} \tag{2}$$

where:

$$g(r) = \text{circ}(r) = 1, \quad |r/a| \leq 1, \\ = 0, \quad \text{otherwise,}$$

$g(r)$  represents the complex amplitude of the fibre,  $a = d_f/2$  is the radius of the fibre. It should be noted that the refraction inside the fibre is neglected since the fibre and the immersion liquid have the same refractive indices ( $\mu_f = \mu_L$ ).  $\Delta$  is the optical path difference between the first two transmitted rays and  $\epsilon$  is the differential increment

introduced in the successive transmitted rays.  $k = 2\pi/\lambda$  is the propagation constant and  $r_1$  is the amplitude reflection coefficient of either of the plates of the interferometer. Equation (2) can be rewritten as follows:

$$U'_1(r) = U_1(r)g(r)\{1 + r_1^2 \exp(jk\Delta)[1 + r_1^2 \exp(jk(\Delta + \varepsilon_1)) + r_1^4 \exp 2jk(\Delta + \varepsilon_2/2) + \dots]\}, \tag{3}$$

$r(x, y)$  is the radial coordinate in the plane of the interferometer assuming that the wedge angle  $\alpha$  is nearly less than  $1^\circ$ .

Assuming that  $\varepsilon_2 = 2\varepsilon_1$ , hence  $U'_1(r)$  becomes

$$U'_1(r) = U_1(r)g(r)\{1 + r_1^2 \exp(jk\Delta)[1 + r_1^2 \exp(jk(\Delta + \varepsilon_1)) + r_1^4 \exp 2jk(\Delta + \varepsilon_1) + \dots]\}. \tag{4}$$

The terms included between the square brackets represent an infinite trigonometric series, *i.e.*,

$$1 + r_1^2 \exp[jk(\Delta + \varepsilon_1)] + r_1^4 \exp[2jk(\Delta + \varepsilon_1)] + \dots = \frac{1}{1 - r_1^2 \exp(jk(\Delta + \varepsilon_1))}. \tag{5}$$

Substituting from Eq. (5) into Eq. (4), we get

$$U'_1(r) = U_1(r)g(r)\left\{1 + \frac{r_1^2 \exp(jk\Delta)}{1 - r_1^2 \exp[jk(\Delta + \varepsilon_1)]}\right\}. \tag{6}$$

Hence, the transmitted complex amplitude becomes

$$U'_1(r) = A_1 \exp[-\pi(r/b_1)^2]g(r)\left\{1 + \frac{r_1^2 \exp(jk\Delta)}{1 - r_1^2 \exp[jk(\Delta + \varepsilon_1)]}\right\}. \tag{7}$$

The Fourier spectrum in the focal plane of the transforming lens  $L_1$  is obtained as

$$\tilde{U}_2(\rho) = \text{F.T.}[U'_1(r)] = \text{F.T.}\left\{A_1 \exp[-\pi(r/b_1)^2]g(r)\left[1 + \frac{r_1^2 \exp(jk\Delta)}{1 - r_1^2 \exp(jk(\Delta + \varepsilon_1))}\right]\right\} \tag{8}$$

where  $\rho = (u, v)$  is the radial coordinate in the Fourier plane. It is clear that the fundamental component of the 1-st transmitted beam is obtained, from Eq. (8), as follows:

$$\tilde{U}_{21}(\rho_{1st}) = \text{F.T.}\{A_1 \exp[-\pi(r/b_1)^2]g(r)\}.$$

Operating the transformation, then we get this result

$$\tilde{U}_{21}(\rho_{1st}) = A_1 \exp-\pi(\rho b_1)^2] * \tilde{g}(\rho) \tag{9}$$

where \* denotes convolution operation, and  $\tilde{g}(\rho) = \text{F.T.}[g(r)]$ .

For the following transmitted beam, we get this result

$$\tilde{U}_{22}(\rho_{2nd}) = A_1 r_1^2 \exp\{-\pi[(\rho - \Delta)b_1]^2\} * \tilde{g}(\rho). \tag{10}$$

Also, we obtain this result for the third transmitted beam

$$\tilde{U}_{23}(\rho_{3rd}) = A_1 r_1^4 \exp\{-\pi b_1^2 [\rho - (2\Delta + \varepsilon_1)]^2\} * \tilde{g}(\rho). \quad (11)$$

Consequently, the overall Fourier spectrum is localized as a series of shifted Gaussian functions represented as follows:

$$\tilde{U}_2(\rho) = \sum_{i=1}^{i=N} \tilde{U}_{2i}(\rho) \quad (12)$$

where  $N$  is the number of the transmitted rays. After having performed Fourier transformations  $\tilde{g}(\rho) = \text{F.T.}[g(r)]$ , the Fourier spectrum of the fibres being considered as an object is

$$\tilde{g}(\rho) = \frac{2J_1(\gamma\rho)}{\gamma\rho} \quad (13)$$

where:  $\gamma = 2\pi a/\lambda f$  is a parameter,  $J_1$  is the Bessel function of the 1st order,  $f$  is the focal length of the Fourier transform lens.

The Fourier components are grouped as in Eq. (12), the complex amplitude in the imaging plane is obtained by operating the Fourier transform upon Eq. (12)

$$\begin{aligned} U_3(r') &= \text{F.T.}\{\tilde{U}_2(\rho)\} \\ &= \text{F.T.}\{A_1 e^{-\pi(\rho/b_1)^2} * [\delta(\rho) + r_1^2 \delta(\rho - \Delta) + r_1^4 \delta(\rho - \Delta - \varepsilon_1) + \dots] * \tilde{f}(\rho)\}. \end{aligned} \quad (14)$$

Solving this transformation, then we finally get

$$U_3(r') = A_1 e^{-\pi(r'/b_1)^2} g(r') \left[ 1 + \frac{r_1^2 e^{jk\Delta}}{1 - r_1^2 e^{jk(\Delta + \varepsilon_1)}} \right]. \quad (15)$$

It is clear that Eq. (15) represents the complex amplitude in the imaging plane ( $r' = x', y'$ ), while Eq. (7) represents the complex amplitude in the object plane ( $r = x, y$ ), as shown in Fig. 1.

The recorded intensity in the imaging plane  $r'(x', y')$  is obtained by taking the modulus square of the complex amplitude  $U_3(r')$  as follows:

$$I(r') = U_3(r') U_3^*(r') = |U_3(r')|^2. \quad (16)$$

For simplicity of calculations, the complex term found in Eq. (15) is multiplied by its complex conjugate to obtain the complex amplitude as follows:

$$\begin{aligned} U_3(r') &= \frac{A_1 e^{-\pi(r'/b_1)^2} g(r')}{[1 + r_1^4 - 2r_1^2 \cos k(\Delta + \varepsilon_1)]} \\ &\times \{1 + r_1^4 - 2r_1^2 \cos[k(\Delta + \varepsilon_1)] + r_1^2 [\cos(k\Delta) - r_1^2 \cos(k\varepsilon_1)] \\ &+ jr_1^2 [\sin(k\Delta) + r_1^2 \sin(k\varepsilon_1)]\}. \end{aligned} \quad (17)$$

Consequently, the recorded intensity becomes

$$I(r') = \frac{A_1^2 \exp[-2\pi(r'/b_1)^2]}{[1 + r_1^4 - 2r_1^2 \cos k(\Delta + \varepsilon_1)]} |g(r')|^2$$

$$\times \{r_1^4 [\sin(k\Delta) + r_1^2 \sin(k\varepsilon_1)]^2 + ([1 + r_1^4 - 2r_1^2 \cos k(\Delta + \varepsilon_1)] + r_1^2 [\cos(k\Delta) - r_1^2 \cos(k\varepsilon_1)])^2\}. \quad (18)$$

This last equation describes the intensity distribution in the imaging plane of a wedge interferometer.

### 2.1. Special case

In the case of a Fabry–Perot interferometer, the optical path difference between any two successive rays is a constant value  $\Delta = 2\mu_L t \cos i'_1$  (where  $i'_1$  – angle of refraction,  $\mu_L$  – refractive index of the interferometric gap, and  $t$  – interferometric gap thickness). The two plates are arranged in parallel, *i.e.*,  $\varepsilon_1$  in Eq. (18) is set equal to zero. Hence we get

$$I(r') = \frac{A_1^2 \exp[-2\pi(r'/b_1)^2]}{[1 + r_1^4 - 2r_1^2 \cos(k\Delta)]} \{[r_1^2 \sin(k\Delta)]^2 + [1 - r_1^2 \cos(k\Delta)]^2\} |g(r')|^2. \quad (19)$$

Consequently, we obtain an expression similar to that of Airy distribution derived in the case of Fabry–Perot interferometer, except that a modulation term is introduced due to both the laser beam and the fibre as follows:

$$I(r') = \frac{A_1^2 \exp[-2\pi(r'/b_1)^2]}{(1 - r_1^2)^2 + 4r_1^2 \sin^2(k\Delta/2)} |g(r')|^2. \quad (20)$$

For uniform illumination and in the absence of any modulation, the ordinary formula of Airy distribution is obtained from Eq. (20) as follows:

$$I(r') = \frac{1}{(1 - r_1^2)^2 + 4r_1^2 \sin^2(k\Delta/2)} \quad (21)$$

where the Gaussian function is replaced by a constant value representing the uniform illumination.

### 2.2. Effect of laser modulation upon the contrast

In this subsection, we show that the contrast of the image is affected by an amplitude modulation of the laser propagating as a Gaussian beam. Hence, referring to the intensity distribution Eq. (20), the local maximum intensity is obtained for  $k\Delta = 2m\pi$ , where  $m = 0, 1, 2, \dots$ , *etc.*, as follows:

$$I_{\max}(r') = A_1^2 \exp[-2\pi(r'/b_1)^2] / [1 - r_1^2]^2, \quad (22)$$

while the local minimum intensity is obtained for  $k\Delta = (2m + 1)\pi$ ;  $m = 0, 1, 2, \dots$ , *etc.*, as follows:

$$I_{\min}(r') = A_1^2 \exp[-2\pi(r'/b_1)^2] / [1 + r_1^2]^2. \quad (23)$$

It is clear that both of the maximum and minimum intensities are dependent on the radial coordinate  $r'$  at certain mirror reflectivity  $r_1$ . Using the visibility definition, the contrast is computed as follows:

$$C_M = [I_{\max}(r') - I_{\min}(r')] / [I_{\max}(r') + I_{\min}(r')]. \quad (24)$$

Substituting from Eqs. (22) and (23) into Eq. (24), hence we get this result for the contrast of the fringes obtained in the case of Gaussian modulation

$$C_M = \frac{1 - \left( \frac{1 - r_1^2}{1 + r_1^2} \right)^2 e^{-2\pi}}{1 + \left( \frac{1 - r_1^2}{1 + r_1^2} \right)^2 e^{-2\pi}} \quad (25)$$

where:

$$I_{\max}(r' = 0) = A_1^2 / (1 - r_1^2)^2$$

and

$$I_{\min}(r' = b) = A_1^2 \exp(-2\pi) / (1 + r_1^2)^2.$$

It is evident that the fringe contrast is dependent upon the reflectivity  $r_1$  of the mirrors but modulated by an exponential decay factor produced due to the manipulation of the Gaussian beam. Contrary to that, in the case of uniform illumination the contrast reduces to the well known expression

$$C = 2r_1^2 / [1 + r_1^4]. \quad (26)$$

Equation (26) is obtained from the original formula of intensity distribution Eq. (20) remembering that the Gaussian distribution is replaced by a constant value or equivalently using Eqs. (21) and (24).

### 2.3. Effect of modulation upon sharpness in the case of Fabry–Perot interferometer

Since the maximum intensity located at the centre of the imaging plane is represented by Eq. (22) as

$$I_{\max}(r') = A_1^2 / [1 - r_1^2], \quad r' = 0,$$

hence, substituting into Eq. (20), we can rewrite the intensity distribution as follows:

$$I(r') = \frac{I_{\max} e^{-2\pi(r'/b_1)^2}}{1 + \frac{4r_1^2}{(1 - r_1^2)^2} \sin^2(k\Delta/2)}. \quad (27)$$

Referring to the definition of half-width  $\delta$ ,  $I/I_{\max} = 1/2$  obtained at the centre of the imaging plane  $r' = 0$ , and solving with respect to  $\delta$ , we finally get this result in the case of Gaussian modulation

$$\delta_M = 2 \sin^{-1} \left\{ \left( \frac{1 - r_1^2}{2r_1} \right) [2e^{-2\pi(r'/b_1)^2} - 1] \right\}, \quad (28)$$

while in the case of uniform illumination, the Gaussian function is replaced by a unity as a constant value in Eq. (28), and we get the ordinary result as follows:

$$\delta = 2 \sin^{-1} \left( \frac{1-r_1^2}{2r_1} \right). \tag{29}$$

It is clear that the modulated half-width  $\delta_M$  is affected by the resultant contribution of both the Gaussian function and the reflectivity of the mirrors.

### 3. Calculation of the optical path difference in a liquid wedge using uncladded fibre of $\mu_f = \mu_L$

Consider a liquid wedge interferometer of wedge angle  $\alpha$  and that uncladded specimen of glass fibre is immersed in a liquid wedge of a refractive index  $\mu_f$  nearly equal to that of the liquid  $\mu_L$ , as shown in Fig. 2.

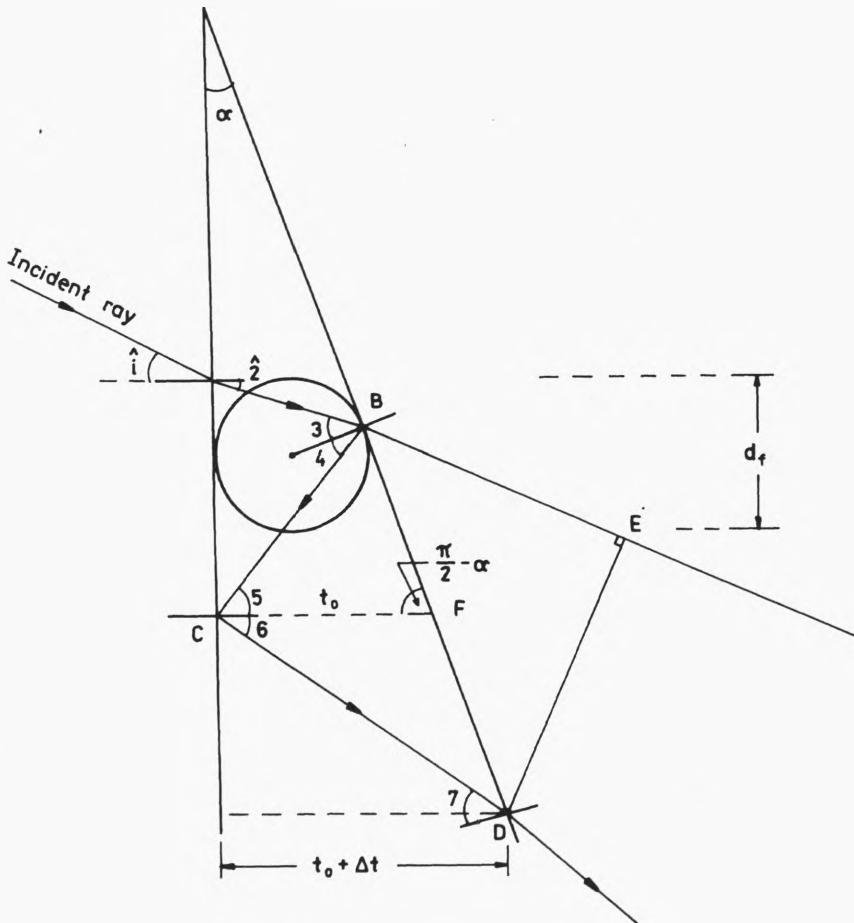


Fig. 2. Optical path difference between rays propagating inside uncladded fibre of circular cross-section, where the refractive index of the liquid wedge  $\mu_L$  is adjusted equal to that of the fibre  $\mu_f$ , i.e.,  $\mu_L = \mu_f$ ,  $\hat{2}$  is the angle of refraction corresponding to the angle of incidence  $\hat{i}$  and  $\hat{\alpha}$  is the wedge angle

Referring to Figure 2, an incident ray making an angle  $i_1$  on the first surface of the interferometer will make a refraction angle  $\hat{2}$  obtained from Snell's law of refraction as follows:

$$\sin \hat{i}_1 = \mu_L \sin(\hat{2}). \quad (30)$$

The optical path difference is calculated as:

$$\text{O.P.D.} = \mu_L(BC + CD) - BE. \quad (31)$$

From the geometry of Fig. 2, it is shown that

$$\hat{3} = \hat{4} = \hat{2} + \hat{\alpha}, \quad \hat{5} = \hat{6} = \hat{2} + 2\hat{\alpha}, \quad \text{and} \quad \hat{7} = \hat{2} + 3\hat{\alpha}. \quad (32)$$

Hence, the reflecting angle on the inclined surface of the wedge  $r_m$  may be represented as follows:

$$\hat{r}_m = \hat{2} + (2n + 1)\hat{\alpha} \quad (33)$$

where  $n = 0, 1, 2, 3, \dots$ , etc., and  $m = 2n + 1$ .

Substituting from Eq. (30) into Eq. (33), we obtain

$$r_m = \sin^{-1} \left( \frac{\sin \hat{i}_1}{\mu_L} \right) + (2n + 1)\hat{\alpha}. \quad (34)$$

In the particular case of parallel arrangement of the plates where  $\alpha$  is set equal to zero, the second term in Eq. (34) is omitted, and we get

$$r_m = \sin^{-1} \left( \frac{\sin \hat{i}_1}{\mu_L} \right). \quad (35)$$

From the geometry of Fig. 2, the optical path difference between the first interfering beams becomes

$$\begin{aligned} \Delta &= \mu_r t_0 \{ [\cos(\alpha)/\cos(\hat{2} + \hat{\alpha})] + \cos(\hat{2} + 2\hat{\alpha}) \\ &\quad - [\tan(\hat{2} + \hat{\alpha}) \sin(\hat{2} + 2\hat{\alpha})] / \cos(\hat{2} + 3\hat{\alpha}) [ \cos(\hat{2} + \hat{\alpha}) + \cos(\hat{2} + 3\hat{\alpha}) ] \\ &\quad + \mu_L \Delta t \cos(\hat{2} + 2\hat{\alpha}) \} \end{aligned} \quad (36)$$

where  $\Delta t = t_0 [\sin(\hat{\alpha}) \sin(\hat{2} + 2\hat{\alpha})] / \cos(\hat{2} + 3\hat{\alpha})$ .

It is clear that the O.P.D. is dependent on the incident angle  $\hat{i}_1$  and the wedge angle  $\hat{\alpha}$ .

#### 4. Theoretical results and discussion

The computational results of Equation (20) are graphically represented as shown in Figs. 3 and 4. The intensity variation versus the optical phase difference are plotted, where five curves are shown as in Fig. 3 for  $r'/b_1 = 0.1, 0.2, 0.3, 0.4$  and  $0.5$ . Another set of four curves is shown as in Fig. 4, where  $r'/b_1 = 0.6, 0.7, 0.8,$  and  $0.9$ . The results represented in both figures are plotted considering Gaussian laser modulation. A curve is plotted as in Fig. 5 taking into account uniform illumination of

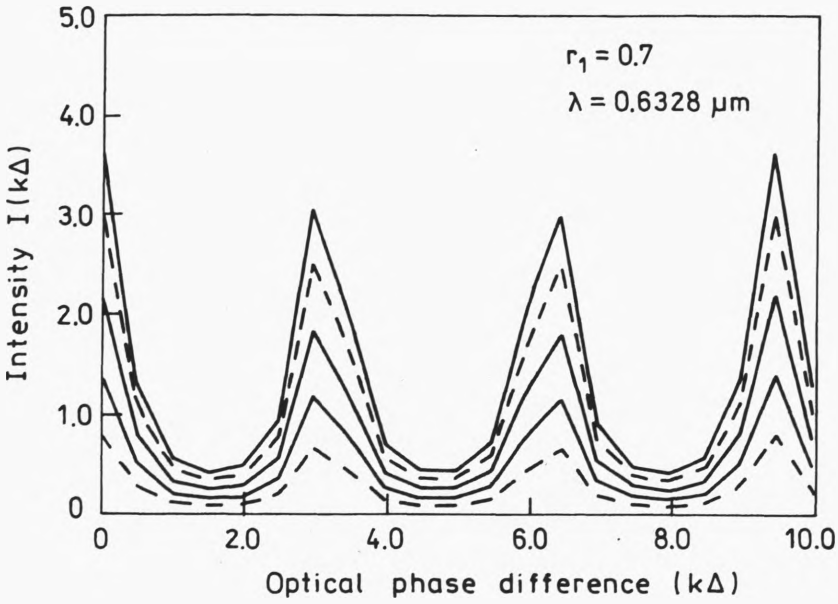


Fig. 3. Intensity  $I(k\Delta)$  versus the optical phase difference in the case of modulated Gaussian function for five different values of  $r'/b_1$ . The upper curve is plotted for  $r'/b_1 = 0.1$  and the following lower curves are plotted for  $r'/b_1 = 0.2, 0.3, 0.4$  and  $0.5$ , respectively

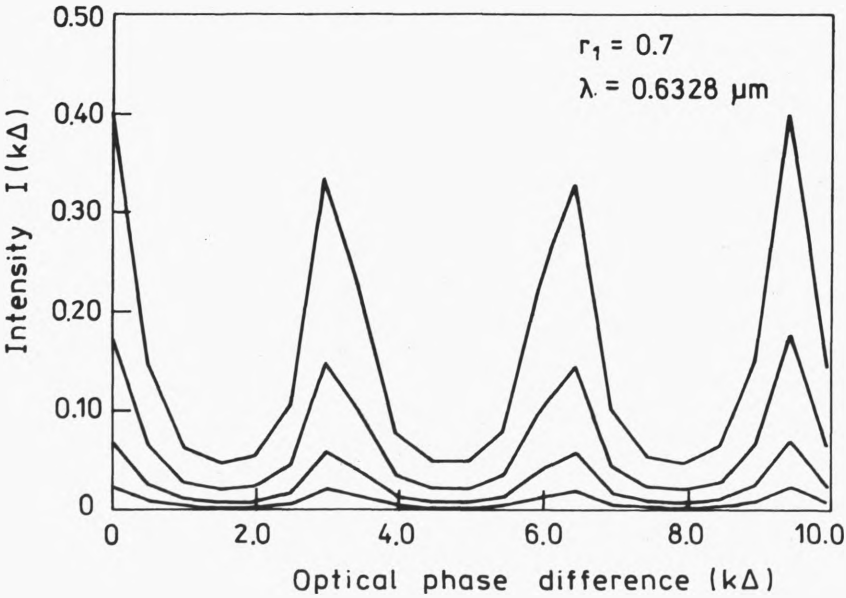


Fig. 4. Intensity  $I(k\Delta)$  versus the optical phase difference in the case of modulated Gaussian function for four different curves of  $r'/b_1 = 0.6, 0.7, 0.8$  and  $0.9$ . The upper curve is plotted for  $r'/b_1 = 0.6$

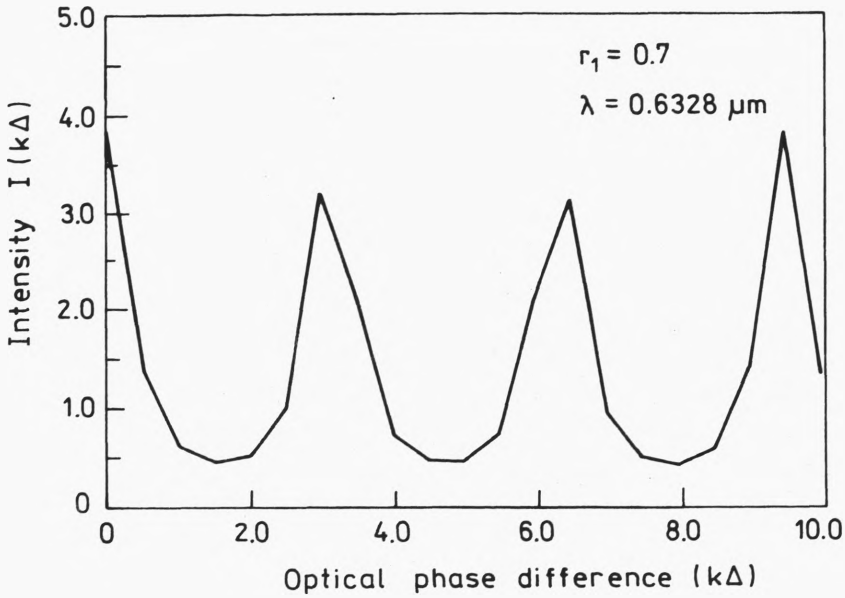


Fig. 5. Intensity  $I(k\Delta)$  versus optical phase difference  $(k\Delta)$  in the case of uniform illumination of the Fabry-Perot interferometer, i.e.,  $(r'/b_1) = 0$

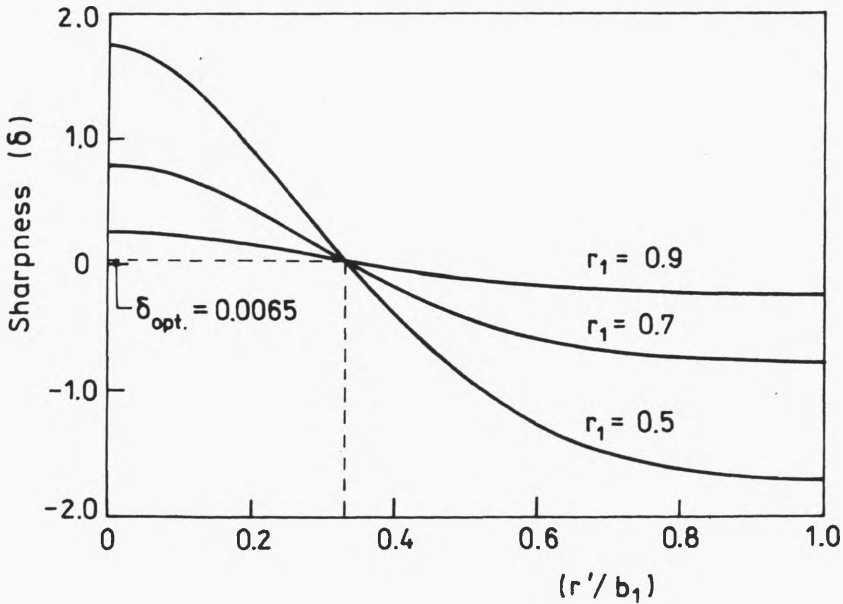


Fig. 6. Sharpness of fringes versus radial imaging coordinate  $(r'/b_1)$  in the case of Gaussian modulation for three different values of reflectivities

Fabry–Perot interferometer (*i.e.*, the case of no modulation using Eq. (21)). All of the above figures are plotted using mirrors of reflectivity  $r_1 = 0.7$ . It is clear from the results obtained that the intensity oscillates between maximum and minimum values occurring at  $k\Delta = 2m\pi$  and  $k\Delta = (2m+1)\pi$ , respectively, where  $m = 0, 1, 2, 3, \dots$ , *etc.* Also, referring to Figs. 3 and 4, the greater intensity peaks occur at lower values of  $r'/b_1$ , *i.e.*, near the centre of the imaging plane. Contrarily, for greater values of  $r'/b_1$  the intensity peaks have lower values due to the presence of Gaussian distribution.

The obtained values of contrast are modulated by an exponential decay factor  $\exp(-2\pi)$  in the case of Gaussian modulation equation (25). It is shown that the contrast  $C_M$  for such a modulation is better than contrast  $C$  obtained with uniform illumination for certain reflectivity  $r_1$ , *e.g.*,  $C_M = 0.9899 > C = 0.7903$  at  $r_1 = 0.7$ . A comparable contrast is attained for higher values of mirror reflectivities, *i.e.*,  $C_M = 0.999$  and  $C = 0.978$  for  $r = 0.9$ . For practical applications it is better to illuminate the interferometer by a laser source having a Gaussian distribution.

Sharpness of fringes versus radial imaging coordinate ( $r'/b_1$ ) is plotted, using Eq. (28), as shown in Fig. 6 for a modulated Gaussian beam. Referring to Eq. (28), the sharpness or half-width is dependent upon both of the mirror reflectivities and the Gaussian distribution of the laser beam. Three curves are plotted for three different values of reflectivities  $r_1 = 0.5, 0.7$  and  $0.9$ , as in Fig. 6. It is clear that the sharpness varies quadratically according to the Gaussian distribution.

The half-width  $\delta_M$  decreases as  $r'/b_1$  until reaching minimum value at  $(r'/b_1) = 0.33$  which may be considered as the optimum sharpness. As a numerical example, in the case of uniform illumination  $\delta = 0.7457$  radians, while  $\delta_M = 0.65$  in the case of Gaussian modulation. In both calculations, we take  $r_1 = 0.7$ . The optimum value  $\delta_{opt} = 0.0065$  radians occurs at  $r'/b_1 = 0.33$  for the same mirror reflectivity  $r_1 = 0.7$ . It is shown that comparable results of sharpness are obtained at higher values of mirror reflectivities and it is better than the obtained values for lower reflectivities, as shown in Fig. 6.

## 5. Conclusions

The theoretical study showed that a modulated Airy distribution, obtained in the case of Fabry–Perot interferometer, is extracted from the intensity distribution of the wedge interferometer. The visibility expression is dependent on both of the reflectivities of the plates and the Gaussian distribution of the beam in the imaging plane. The contrast is improved in the case of Gaussian modulation as compared with that obtained in the case of uniform illumination.

## References

- [1] TOLANSKY S., *Surface Microtopography*, Longmans Green, London 1960.
- [2] BORN M., WOLF E., *Principles of Optics*, Pergamon Press, Oxford, London 1964.
- [3] BARAKAT N., MOKHTAR S., *J. Opt. Soc. Am.* **53** (1963), 159.

- [4] BARAKAT N., HAMZA A., *Interferometry of Fibrous Materials*, Adam Hilger, Ltd. Techno House, Bristol 1990.
- [5] BARAKAT N., *Textile Res. J.* **41** (1971), 167.
- [6] EL NICKLAWY M. M., FOU DA I. M., *Textile Res. J.* **71** (1980), 252.
- [7] HAMZA A., SOKKAR T. Z. N., KABEEL M. A., *J. Phys. D: Appl. Phys.* **19** (1986), 119.
- [8] HAMZA A., SOKKAR T. Z. N., KABEEL M. A., *J. Phys. D: Appl. Phys.* **18** (1985), 1773.
- [9] BARAKAT N., EL HENNAWI H. A., *Textile Res. J.* **41** (1971), 391.
- [10] BARAKAT N., HINDELAH A. M., *Textile Res. J.* **41** (1964), 581.
- [11] FOU DA I. M., EL NICKLAWY M. M., *Acta Phys. Pol., A* **59** (1981), 95.
- [12] HAMZA A., SOKKAR T. Z. N., SHAHIN M. M., *J. Microsc.* **137** (1985), 85.
- [13] BARAKAT N., HAMZA A., GONEID A., *Appl. Opt.* **24** (1985), 4383.
- [14] HAMZA A., SOKKAR T. Z. N., KABEEL M. A., *J. Phys. D: Appl. Phys.* **18** (1985), 2321.
- [15] BOGGS L. M., PRESBY H. M., MARCUSE D., *Bell Syst. Tech. J.* **58** (1979), 867.
- [16] PRESBY H. M., MARCUSE D., ASTLE H. W., BOGGS L. M., *Bell Syst. Tech. J.*, **58** (1979), 883.
- [17] GASKILL J. D., *Linear Systems, Fourier Transform and Optics*, Wiley and Sons Inc., New York 1978.

*Received May 22, 1997  
in revised form August 6, 1997*